Received 26 December 2023; accepted 15 January 2024. Date of publication 26 January 2024; date of current version 13 February 2024.

Digital Object Identifier 10.1109/OJCOMS.2024.3358057

Performance Analysis of Two-Way Relaying in mmWave-Based Aerial Links

HEYAM F. HASSAN[1], SAUD ALTHUNIBAT[1,2] (Senior Member, IEEE), MOHAMMAD TAGHI DABIRI[3], MAZEN HASNA[3] (Senior Member, IEEE), AND KHALID A. QARAQE[1] (Senior Member, IEEE)

[1]Department of Electrical and Computer Engineering, Texas A&M University at Qatar, Doha, Qatar

[2]Department of Communications Engineering, Al-Hussein Bin Talal University, Maan, Jordan

[3]Department of Electrical Engineering, Qatar University, Doha, Qatar

CORRESPONDING AUTHOR: H. F. HASSAN (e-mail: heyam.hassan@qatar.tamu.edu)

Open Access funding provided by the Qatar National Library. This publication was made possible by NPRP14C-0909-210008 from the Qatar National Research Fund (a member of The Qatar Foundation).

ABSTRACT Two-Way Relaying (TWR) is an efficient relaying technique that doubles the spectral efficiency as compared to the traditional one-way relaying. As such, it has been nominated as a solution to extend the coverage of links operating on the Millimeter Wave (mmWave) band. In this paper, the performance of TWR is investigated for mmWave-based aerial links in which the involved entities are all aerial. Taking into account the orientation fluctuations of the involved aerial entities, the performance is characterized in terms of the outage rate and the bit error rate. Closed form expressions are derived based on the considered performance metrics along with a large set of Monte Carlo simulations results to validate the obtained analytical formulas. Analytical and simulation results address the impact of various factors including the number of antenna elements, the modulation order, the transmission distance, and fluctuation intensity.

INDEX TERMS Relaying systems, millimeter wave band, two-way relaying, unmanned aerial vehicle.

I. INTRODUCTION

THE ADVANCEMENT of wireless networks requires integrating high-frequency spectrum to handle the increasing number of connected devices and data demands. To meet these requirements, millimeter wave (mmWave) bands have emerged as a promising solution, offering ample bandwidth and faster data rates compared to microwave bands [1]. However, mmWave faces challenges in non-line-of-sight (NLoS) scenarios due to obstacles and signal loss [2]. Another challenge that is usually reported in the mmWave bands is the shorter transmission distances as compared to other lower RF bands. To this end, multi-hop links can be utilized where two nodes exchange data with the help of a relay node, allowing efficient and reliable data transmission even in obstructed environments [3]. Two common relaying strategies are popularly used in the literature, namely, one-way relaying (OWR) and two-way relaying (TWR). In OWR, the relay assists in transmitting data from a source node to a destination node. The relay receives the signal from the source, processes it, and then forwards it to the destination. Two more time slots are needed for transmitting in the opposite direction. In TWR, both source nodes communicate simultaneously with the relay, which processes and broadcasts the received signals back to the source nodes. This bidirectional communication in TWR improves spectral efficiency and enables more flexible information exchange [4]. Relaying schemes include decode-and-forward (DF), where the relay decodes and re-encodes data, and amplify-and-forward (AF), where the relay amplifies data without decoding [5].

Although relays can efficiently boost the link performance and maintain the signal strength acceptable at the destination, their performance over mmWave still subject to the line-of-sight (LoS) requirement which might be unavailable via terrestrial entities. To this end, unmanned aerial vehicles (UAVs) can play a significant role in attaining the LoS for both communication ends due to their mobility, flexibility and adaptability [3]. UAVs can efficiently cover large areas, making them valuable for communication in emergencies cases when terrestrial infrastructure is compromised [6].

Moreover, they can operate in hazardous environments, making them suitable for rescue missions. Integrating UAVs in mmWave-based multi-hop networks has gained significant attention due to its potential to revolutionize wireless communication systems. This combination results in a robust and adaptable communication system that enhances the overall performance and reliability of wireless networks ensuring continues connection during critical situations [7].

In spite of the significant research conducted on UAV-based multi-hop networks, a distinct gap remains in the literature regarding the exploration of TWR air-to-air communication utilizing mmWave bands. Literature studies have not sufficiently tackled the effect of the random fluctuations of the UAV's antennas on the performance of the overall link. One of the challenges in aerial links involves the use of hovering UAVs, which are sensitive to continuous vibrations. These vibrations directly impact the performance due to the resulting fluctuations of the antennas. Moreover, the conventional TWR scheme is not applicable in mmWave due to the use of directional antennas, preventing simultaneous service to nodes with the same antenna. To this end, in this work, the performance of TWR in mmWave-based aerial links is investigated, which has never been addressed to the best of our knowledge. The primary contributions of this work can be summarised as follows:

- The channel model for aerial links is developed by considering the antenna propagation patterns specified in the 3GPP standards, angular antennas fluctuations, path loss and channel fading.
- A comprehensive mathematical framework is followed aiming to obtain closed-form expressions for the bit error rate (BER) and the outage probability (OP) in the TWR mmWave-based aerial links.
- Extensive simulation results of the considered system is presented to validate and corroborate the analytical findings.
- The system performance is thoroughly studied by exploring various parameters, including modulation order, the separation distance, UAV's instability parameter, and the number of antenna elements.

The rest of this paper is organized as follows. Related works are presented in Section II. Section III outlines the system model and the formulation of the antennas' gain. Further details into the TWR mmWave-based aerial link include transmission and relaying phases are discussed in Section IV. In Section V, the performance analysis of the investigated system covering BER analysis and OP analysis is presented. The validation of the derived analytical formulas through simulation results is illustrated in Section VI. Finally, conclusion presented in Section VII.

II. RELATED WORK

In the literature, there is a set of related works that investigates the performance of mmWave based TWR links. In [8], authors discuss the advantages of using AF-TWR in a mmWave network for bi-directional data exchange between two end users. A relay-selection approach is presented to optimize signal quality, coverage, and spectral efficiency. The work in [9] investigates beamforming design for improving secrecy capacity in mmWave TWR networks, where iterative algorithms are employed to efficiently solve the beamforming problem, and numerical experiments are presented to validate the effectiveness of the proposed designs in enhancing security. In addition, a study on mmWave TWR systems for advanced cellular networks is presented in [10]. The approach studied addresses challenges related to self-interference and sparse mmWave channels, and extensive simulations confirm the algorithm's effectiveness in reducing error rate.

Recently, several works have addressed the performance of the UAVs in various communication systems. A UAV-assisted TWR networks for data exchange is investigated in [11] considering two methods; full-duplex and half-duplex. Optimizing bandwidth and power allocation in both cases is shown to be a complex problem, where approximations are presented which reveal that the half-duplex approach is more efficient than the full-duplex. Authors in [12] focus on a UAV-assisted TWR system using a two-slot network coding scheme and an iterative algorithm is introduced to maximize the system's average sum rate along with examination of the impact of traffic patterns on performance. Results demonstrate that a moving relay system offers higher throughput compared to a static relay. Authors in [13] explore a UAV-based multi-hop TWR network with multiple UAVs assisting two ground users in information exchange. The proposed pattern achieves a data rate of (1/2) data packets per time slot, marking a notable enhancement in throughput compared to alternative schemes. The research in [14] concentrates on a TWR system, formulating achievable secrecy energy-efficiency by considering various UAV parameters. The problem is solved iteratively through decomposition and optimization techniques, and simulation results show that the proposed methods outperform existing approaches. In [15], an extensive investigation of a cooperative UAV network is demonstrated, employing a two time slots transmission approach, a half-duplex mode, and a DF protocol. Closed-form expressions for both end-to-end Signal-to-Noise Ratio (SNR) and OP are derived. Additionally, Monte Carlo simulations are employed to study the impact of various factors on the OP. In [16], a study is conducted to investigate mmWave-based D2D communication under Nakagami-m fading channels. The OP for D2D users with interference from multiple cellular is analyzed. The study takes into consideration sectorized beamforming gain probabilities and distance from interfering nodes. The results indicate that the D2D OP decreases with higher main lobe gain and increases with higher side lobe gain.

To the best of our knowledge, there are no previous works investigating the TWR performance in mmWave-based aerial links. As mentioned earlier, integrating aerial entities in multi-hop links affects the performance due to the fluctuations of the antennas orientation, which, in turn, results in a performance degradation in both OP and BER.

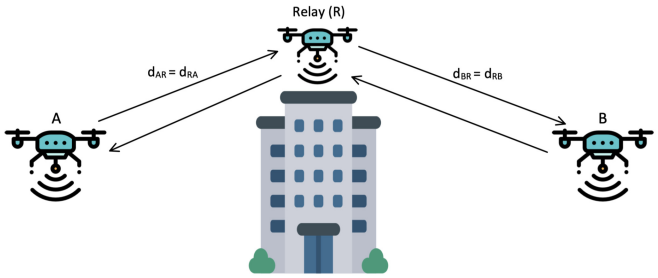

FIGURE 1. The considered system of TWR mmWave-based aerial link.

FIGURE 2. UAVs' antennas misalignment in a dual-hop mmWave-based aerial link.

III. SYSTEM MODEL

The system under consideration involves three hovering UAVs, particularly quadrotor. Quadrotor UAVs are capable of remaining stationary and flying at zero-speed [17], [18], [19], [20], [21], [22]. The considered UAVs utilizing mmWave frequencies to establish communication between each other. Among these UAVs, one serves as a relay ($\mathcal{R}$) positioned between the other two UAV nodes $\mathcal{A}$ and $\mathcal{B}$, as depicted in Fig. 1. Both source nodes communicate simultaneously with the relay. The relay operates in a DF mode, where it decodes the received data before forwarding it to the destination node. Note that the direct communication link between nodes $\mathcal{A}$ and $\mathcal{B}$ is not available due to obstacles, or high path loss. The modulators of the nodes are considered to use the same modulation order, denoted by M. The signals transmitted from nodes $\mathcal{A}$, $\mathcal{B}$, and $\mathcal{R}$ are affected by the channel fading, and path loss. Nodes $\mathcal{A}$ and $\mathcal{B}$ are equipped with single uniform square array antennas, serving for both transmission and reception tasks. In contrast, relay node $\mathcal{R}$ is equipped with a dual-antenna configuration, each antenna is dedicated to separately serve nodes $\mathcal{A}$ and $\mathcal{B}$ which are assumed to be sufficiently spaced.

As illustrated in Fig. 2, operating within a hovering UAVs system introduces the challenge of vibrations stemming from internal or external factors. These vibrations lead to dynamic shifts in the positions and orientations of the antennas on nodes $\mathcal{A}, \mathcal{B}$ and $\mathcal{R}$. These fluctuations exert a significant influence on the directional mmWave links, thereby highlighting their pivotal role in shaping the link's overall performance. These fluctuations manifest as angular deviations in both x and y directions, denoted by $\theta_k = (\theta_{kx}, \theta_{ky})$. These angles follow a Gaussian distribution, with $\theta_{kx} \sim \mathcal{N}\ \{\theta'_{kx}, \sigma^2_{\theta x}\}$ and $\theta_{ky} \sim \mathcal{N}\ \{\theta'_{ky}, \sigma^2_{\theta y}\}$, where $k \in \{\mathcal{A}, \mathcal{B}, \mathcal{R}\}$, and σ^2_θ is the UAV's fluctuation intensity.

Each antenna consists of $N \times N$ elements spaced by $\frac{\lambda}{2}$ in both x, and y directions, with an antenna gain denoted as G_k. Note that λ is the antenna wavelength and it is equal to $\lambda = \frac{c}{f_c}$, where c is the speed of light, and f_c is the carrier frequency. Node k's array radiation can be formulated in the direction of θ_k, and ϕ_k as follows [17]

$$\theta_k = \tan^{-1}\left(\sqrt{\tan^2\theta_{kx} + \tan^2\theta_{ky}}\right)$$
$$\phi_k = \tan^{-1}\left(\frac{\tan\theta_{kx}}{\tan\theta_{ky}}\right). \quad (1)$$

These angles, represented in (1), play an important role in defining the antenna gain at node k, i.e., G_k, as follows

$$G_k = G_o G_e G_a, \quad (2)$$

where G_e corresponds to the radiation pattern of an individual antenna element, and G_a represents the antenna array factor. G_o can be determined through the following expression [17]

$$G_o = \frac{1}{\int_0^{\pi}\int_0^{2\pi} G_e G_a \sin(\theta_k)\, d\theta_k d\phi_k}. \quad (3)$$

The exact form of G_e can be inferred from the 3GPP report as follows [23].

$$G_e = 10^{\frac{G_{e,3dB}}{10}}, \quad (4)$$

where $G_{e,3dB}$ can be defined as follows [23]

$$G_e = G_{max} - \min\left\{-\left(G_{e,3dB,1} + G_{e,3dB,2}\right), F_m\right\}, \quad (5)$$

$$G_{e,rdB,1} = -\min\left\{12\left(\frac{\theta_e - 90}{\theta_{e3dB}}\right)^2, G_{SL}\right\}, \quad (6)$$

$$G_{e,rdB,2} = -\min\left\{12\left(\frac{\phi_k}{\phi_{e3dB}}\right)^2, F_m\right\}, \quad (7)$$

$$\theta_e = \arctan\left(\frac{\sqrt{1 + \sin^2(\theta_{ky})}}{\sin(\theta_{ky})}\right), \quad (8)$$

where the maximum directional gain of the antenna element, identified as $G_{\max}$, which is fixed to 10 dBi. Additionally, F_m represents the front-to-back ratio, set to 30 [17]. The side-lobe level limit, denoted as $G_{\rm SL}$, is also set at 30 [17]. The vertical and horizontal 3D bandwidths are represented by $\theta_{e3dB} = 65°$ and $\phi_{e3dB} = 65°$, respectively [17].

The array factor G_a of the square array antenna at node k with dimensions $N \times N$, can be formulated as follows [24]

$$G_a = \left(\frac{\sin\left(N\frac{\pi}{2}\sin(\theta_k)\cos(\phi_k)\right)}{N\sin\left(N\frac{\pi}{2}\sin(\theta_k)\cos(\phi_k)\right)}\right)^2 \times \left(\frac{\sin\left(N\frac{\pi}{2}\sin(\theta_k)\sin(\phi_k)\right)}{N\sin\left(N\frac{\pi}{2}\sin(\theta_k)\sin(\phi_k)\right)}\right)^2. \quad (9)$$

It is worth emphasizing that the array factor G_a remains consistent across all antennas, implying that it exhibits an identical pattern for each antenna. However, its magnitude can vary based on the direction.

Hence, the instantaneous SNR γ_{kl} can be expressed as follows

$$\gamma_{kl} = \frac{P|\eta|^2 \rho_{kl} \mathbb{G}_{kl}}{\sigma^2}, \quad (10)$$

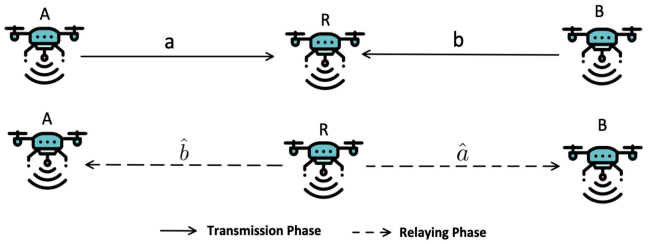

FIGURE 3. Transmission and relaying phases.

where $kl \in \{\mathcal{AR}, \mathcal{RB}, \mathcal{BR}, \mathcal{RA}\}$ represents different links pairs, $\mathbb{G}_{kl} = G_k G_l$ is the overall gain, P denotes the transmit power, η stands for the small-scale fading, σ^2 signifies the noise power, and ρ_{kl} represents the path loss which can be defined based on the 3GPP report as follows [25]

$$\begin{aligned}\rho_{kl} = {} & 20\log_{10}(40\pi(d_{kl})(f_c/3)) \\ & + min(0.03\,h^{1.72}, 10)\log_{10}(d_{kl}) \\ & - min(0.044\,h^{1.72}, 14.77) + 0.002\log_{10}(h)d_{kl}. \quad (11)\end{aligned}$$

The parameter d_{kl} signifies the link distance between k and l, and h represents the average height of the buildings. To account for the channel fading, Nakagami-m model is utilized, where η is Nakagami random variable (RV). As a result, the probability density function (pdf) of the RV $\zeta = |\eta|^2$, denoted as $f_\zeta(\zeta)$, can be formulated as outlined in [26].

$$f_\zeta(\zeta) = \frac{m^m \zeta^{m-1}}{\Gamma(m)} exp(-m\zeta), \quad \zeta > 0, \quad (12)$$

where m is the Nakagami fading parameter, and $\Gamma(\cdot)$ represents the Gamma function.

IV. TWR MMWAVE-BASED AERIAL LINKS

The considered TWR mmWave-based aerial communication system involves two phases carried out across two consecutive time slots, as illustrated in Fig. 3. The first phase is the transmission phase, followed by the relaying phase.

A. TRANSMISSION PHASE

During the transmission phase, each of the nodes $\mathcal{A}$ and $\mathcal{B}$ transmits a symbol to the relay within the first time slot. Specifically, node $\mathcal{A}$ transmits a bit vector denoted as $\mathbf{a}$, containing $\log_2 M$ bits. Similarly, node $\mathcal{B}$ has its own bit vector $\mathbf{b}$ of the same length. These bit vectors, $\mathbf{a}$ and $\mathbf{b}$, modulated through an M-ary modulator at their respective nodes, generating modulated symbols $x_{\mathcal{AR}}$ at node $\mathcal{A}$ and $x_{\mathcal{BR}}$ at node $\mathcal{B}$. Note that all nodes are sufficiently spaced, and antennas are directed toward the respective nodes to prevent mutual interference between the transmitter and receiver. The received signal at the relay node $\mathcal{R}$ from node k upon accomplishing the first phase is $y_{k\mathcal{R}}$, where $k\mathcal{R} \in \{\mathcal{AR}, \mathcal{BR}\}$, and it can be expressed as follows

$$y_{k\mathcal{R}} = \sqrt{P \times \rho_{k\mathcal{R}} \times \mathbb{G}_{k\mathcal{R}}}\, \eta_{k\mathcal{R}}\, x_{k\mathcal{R}} + w_{\mathcal{R}}, \quad (13)$$

where $w_{\mathcal{R}}$ the additive white Gaussian noise at node $\mathcal{R}$. The considered system employs the Maximum Likelihood (ML) detection method, assuming that the channel state information is available at the receiver end. It is noteworthy that ML is considered the optimal detection method [27]. In this phase, the relay node employs ML detection to detect symbols from nodes $\mathcal{A}$ and $\mathcal{B}$ separately, as follows

$$\left[\tilde{x}_{k\mathcal{R}}\right] = \arg \min_{x_{k\mathcal{R}} \in \mathcal{X}} \left| y_{k\mathcal{R}} - \sqrt{P \times \rho_{k\mathcal{R}} \mathbb{G}_{k\mathcal{R}}}\, \eta_{k\mathcal{R}}\, x_{k\mathcal{R}} \right|^2, \quad (14)$$

where $\mathcal{X}$ corresponds to the potential set of $x_{k\mathcal{R}}$, and $|\cdot|$ denotes the norm operator. The resulting bit vectors obtained from the detected symbols at $\mathcal{R}$ are represented by $\hat{\mathbf{a}}$ and $\hat{\mathbf{b}}$ from nodes $\mathcal{A}$ and $\mathcal{B}$, respectively.

B. RELAYING PHASE

Upon completing the transmission phase, the relay proceeds to modulate the decoded symbols for subsequent transmission to nodes $\mathcal{A}$ and $\mathcal{B}$. The received signal at node l from the relay can be mathematically formulated as follows

$$y_{\mathcal{R}l} = \sqrt{P \times \rho_{\mathcal{R}l} \times \mathbb{G}_{\mathcal{R}l}}\, \eta_{\mathcal{R}l}\, x_{\mathcal{R}l} + w_l, \quad (15)$$

where $l \in \{\mathcal{A}, \mathcal{B}\}$. Nodes $\mathcal{A}$ and $\mathcal{B}$ will utilize ML detection on the received signal $y_{\mathcal{R}l}$ to decode the received data as follows

$$\left[\tilde{x}_{\mathcal{R}l}\right] = \arg \min_{x_{\mathcal{R}l} \in \mathcal{X}} \left| y_{\mathcal{R}l} - \sqrt{P \times \rho_{\mathcal{R}l} G_{\mathcal{R}l}}\, \eta_{\mathcal{R}l} x_{\mathcal{R}l} \right|^2. \quad (16)$$

After completing the second phase, each of the nodes has received a symbol from the other node, and the detected bit vectors at nodes $\mathcal{A}$ and $\mathcal{B}$ are denoted as $\hat{\hat{\mathbf{a}}}$ and $\hat{\hat{\mathbf{b}}}$, respectively.

V. PERFORMANCE ANALYSIS

In this section, we will comprehensively evaluate the performance of the investigated scheme using two important measures, namely, BER analysis and OP.

A. BIT ERROR RATE ANALYSIS

Considering the studied system described earlier, it is crucial to note that the average BER at both nodes $\mathcal{A}$ and $\mathcal{B}$ is identical. This uniformity arises because both nodes share identical average channel characteristics, path loss models, antenna gains, and separation distances. Hence, the BER analysis can be limited to only one of the nodes, such as node $\mathcal{B}$. When node $\mathcal{B}$ receives bit sequence, denoted as $\hat{\hat{\mathbf{a}}}$, from node $\mathcal{A}$ through the relay $\mathcal{R}$, the average BER at node $\mathcal{B}$ in the data originating from node $\mathcal{A}$, referred to as $\text{BER}_{\mathcal{AB}}$, can be mathematically expressed as follows

$$\begin{aligned}\text{BER}_{\mathcal{AB}} &= \Pr.\left(\hat{\hat{\mathbf{a}}} \neq \mathbf{a}\right) \\ &= \Pr.\left(\hat{\mathbf{a}} \oplus \mathbf{e}_{\mathcal{RB}} \neq \mathbf{a}\right) \\ &= \Pr.(\mathbf{a} \oplus \mathbf{e}_{\mathcal{AR}} \oplus \mathbf{e}_{\mathcal{RB}} \neq \mathbf{a}) \\ &= \Pr.(\mathbf{e}_{\mathcal{AR}} \oplus \mathbf{e}_{\mathcal{RB}} \neq \mathbf{0}), \quad (17)\end{aligned}$$

where $\mathbf{e}_{\mathcal{AR}}$ and $\mathbf{e}_{\mathcal{RB}}$ represent the error vectors corresponding to the data transmitted from node $\mathcal{A}$ to the relay $\mathcal{R}$,

and from the relay $\mathcal{R}$ to node $\mathcal{B}$, respectively. Each bit in these error vectors can take a value of either 1, indicating an incorrect reception, or 0, indicating a successful reception. Eq. (17) is derived by incorporating different expressions for $\hat{\hat{\mathbf{a}}}$ and $\hat{\mathbf{a}}$, both of which involve these error vectors. The last line in (17) highlights that the situation where $\mathbf{e}_{\mathcal{AR}} \oplus \mathbf{e}_{\mathcal{RB}} \neq \mathbf{0}$ arises exclusively when the bits within the error vectors differ. This condition can be expanded as follows

$$\begin{aligned}\text{BER}_{\mathcal{AB}} = &\Pr.(e_{\mathcal{AR}} = 1 \ \cap \ e_{\mathcal{RB}} = 0) \\ &+ \Pr.(e_{\mathcal{AR}} = 0 \ \cap \ e_{\mathcal{RB}} = 1). \end{aligned} \tag{18}$$

Taking into consideration the independent nature of the error events $e_{\mathcal{AR}}$ and $e_{\mathcal{RB}}$, (18) can be simplified as follows

$$\begin{aligned}\text{BER}_{\mathcal{AB}} = &\Pr.(e_{\mathcal{AR}} = 1)\Pr.(e_{\mathcal{RB}} = 0) \\ &+ \Pr.(e_{\mathcal{AR}} = 0)\Pr.(e_{\mathcal{RB}} = 1). \end{aligned} \tag{19}$$

Let us consider $\alpha_{\mathcal{AR}} = \Pr.(e_{\mathcal{AR}} = 1)$, and $\alpha_{\mathcal{RB}} = \Pr.(e_{\mathcal{RB}} = 1)$. These terms can now be utilized to reformulate (19) as follows

$$\text{BER}_{\mathcal{AB}} = (\alpha_{\mathcal{AR}} + \alpha_{\mathcal{RB}}) - 2(\alpha_{\mathcal{AR}}\alpha_{\mathcal{RB}}), \tag{20}$$

where $\alpha_{\mathcal{AR}}$ and $\alpha_{\mathcal{RB}}$ represent the probabilities of incorrectly decoding the received bit vector at $\mathcal{R}$ from $\mathcal{A}$ and the received bit vector at $\mathcal{B}$ from $\mathcal{R}$, respectively. For a coherent PSK modulation scheme, the average BER over a fading channel for the link $\mathcal{A} - \mathcal{R}$ can be expressed as follows [28]

$$\alpha_{\mathcal{AR}} = \frac{\delta}{2}\int_0^{\infty} \left(1 - \text{erf}\left(\sqrt{\varpi\,\gamma_{\mathcal{AR}}}\right)\right) f_{\gamma_{\mathcal{AR}}}(\gamma)\, d\gamma_{\mathcal{AR}}. \tag{21}$$

where $\text{erf}(\cdot)$ is the error function, $\gamma_{\mathcal{AR}}$ is the instantaneous SNR of the $\mathcal{A} - \mathcal{R}$ link. δ and ϖ can be determined respectively as follows

$$\delta = \begin{cases} 1, & \text{if } M = 2 \\ \frac{2}{log_2 M}, & \text{if } M > 2, \end{cases} \tag{22}$$

and

$$\varpi = \begin{cases} 1, & \text{if } M = 2 \\ \sin^2\left(\frac{\pi}{M}\right), & \text{if } M > 2. \end{cases} \tag{23}$$

The pdf $f_{\gamma_{\mathcal{AR}}}(\gamma)$ in (21) is the pdf of $\gamma_{\mathcal{AR}}$ and it can be computed as follows [17]

$$f_{\gamma_{\mathcal{AR}}}(\gamma) = \sum_{i=0}^{kD-1}\sum_{j=0}^{kD-1} \mathbb{R}_{ij}\gamma_{\mathcal{AR}}^{m-1}\exp(-\mu_{\mathcal{AR}}\gamma_{\mathcal{AR}}), \tag{24}$$

where D is considered as the number of antenna sectors assumed. While $\mathbb{R}_{ij}$ can be expressed as follows

$$\mathbb{R}_{i,j} = \frac{\mathbb{J}_{i,j}\left(\theta'_{\mathcal{A},xy}, \theta'_{\mathcal{R},xy}, \sigma^2_{\theta_{\mathcal{A}}}, \sigma^2_{\theta_{\mathcal{R}}}\right)}{\Gamma(m)}\,\mu_{\mathcal{AR}}^{m}$$

$$\mathbb{J}_{i,j}\left(\theta'_{\mathcal{A}xy}, \theta'_{\mathcal{R}xy}, \sigma^2_{\theta_{\mathcal{A}}}, \sigma^2_{\theta_{\mathcal{R}}}\right) = J_i\left(\theta'_{\mathcal{A}xy}, \sigma^2_{\theta_{\mathcal{A}}}\right) J_j\left(\theta'_{\mathcal{R}xy}, \sigma^2_{\theta_{\mathcal{R}}}\right)$$

$$J_i\left(\theta'_{\mathcal{A}xy}, \sigma^2_{\theta_{\mathcal{A}}}\right) = M\left(\frac{\theta'_{\mathcal{A}xy}}{\sigma_{\theta_{\mathcal{A}}}}, \frac{i}{DN\sigma_{\theta_{\mathcal{A}}}}\right) - M\left(\frac{\theta'_{\mathcal{A}xy}}{\sigma_{\theta_{\mathcal{A}}}}, \frac{i+1}{DN\sigma_{\theta_{\mathcal{A}}}}\right)$$

$$J_i\left(\theta'_{\mathcal{R}xy}, \sigma^2_{\theta_{\mathcal{R}}}\right) = M\left(\frac{\theta'_{\mathcal{R}xy}}{\sigma_{\theta_{\mathcal{R}}}}, \frac{j}{DN\sigma_{\theta_{\mathcal{R}}}}\right) - M\left(\frac{\theta'_{\mathcal{R}xy}}{\sigma_{\theta'_{\mathcal{R}}}}, \frac{j+1}{DN\sigma_{\theta_{\mathcal{R}}}}\right),$$

where μ_{AR} can be expressed as follows

$$\mu_{AR} = \frac{m\sigma^2}{P\,\rho_{\mathcal{AR}}\,\mathbb{R}'_{ij}}, \tag{25}$$

and $\mathbb{R}'_{i,j}$ in (25) can be calculated as follows

$$\mathbb{R}'_{i,j} = \begin{cases} \mathbb{R}'_{i,j} = 4\pi^4\left(G''_o(N)\right)^2 & \text{for } i = 0, j = 0 \\ \mathbb{R}'_{i,j} = 4\left(G''_o(N)\right)^2 \frac{D^4\left(\sin^2\left(\frac{i\pi}{2D}\right)\sin^2\left(\frac{j\pi}{2D}\right)\right)}{i^2 j^2} & \text{for } i \neq 0, j \neq 0 \\ \mathbb{R}'_{i,j} = 2\pi^2\left(G''_o(N)\right)^2 \frac{D^2\left(1-\cos^2\left(\frac{i\pi}{D}\right)\right)}{i^2} & \text{for } i \neq 0, j = 0 \\ \mathbb{R}'_{i,j} = 2\pi^2\left(G''_o(N)\right)^2 \frac{D^2\left(1-\cos^2\left(\frac{j\pi}{D}\right)\right)}{j^2} & \text{for } i = 0, j \neq 0, \end{cases}$$

where $G_o^{(N)}$ can be expressed as follows

$$G_o^{(N)} = 0.2025 \times 10^{\frac{G_{max}}{10}} G_o(N). \tag{26}$$

Accordingly, (21) can be rewritten as follows

$$\alpha_{\mathcal{AR}} = \frac{\delta}{2}\left(1 - \sum_{i=0}^{kD-1}\sum_{j=0}^{kD-1} \mathbb{R}_{ij} \times \int_0^{\infty} \text{erf}\left(\sqrt{\varpi\,\gamma_{\mathcal{AR}}}\right)\gamma_{\mathcal{AR}}^{m-1} \times \exp(-\mu_{\mathcal{AR}}\gamma_{\mathcal{AR}}) \cdot d_{\gamma_{\mathcal{AR}}}\right). \tag{27}$$

The integral appearing in (27) can be evaluated using the formula provided in [29, eq. (4.3.8)]. Consequently, $\alpha_{\mathcal{AR}}$ can be expressed in a closed-form expression as demonstrated in (28), shown at the bottom of the page. Here, ${}_2F_1(.;.;.)$ refers to the hypergeometric Gauss function.

Employing a similar approach as in (21)-(28), a closed-form expression for α_{RB} can also be derived, as shown in (29), shown at the bottom of the page. With these results in hand, the average $\text{BER}_{\mathcal{AB}}$ can be computed by substituting the expressions for $\alpha_{\mathcal{AR}}$ and $\alpha_{\mathcal{RB}}$ from (28) and (29) into (20).

$$\alpha_{\mathcal{AR}} = \frac{\delta}{2}\left(1 - 2\sum_{i=0}^{kD-1}\sum_{j=0}^{kD-1} \mathbb{R}_{ij}\sqrt{\frac{\varpi}{\pi}}\,\mu_{\mathcal{AR}}^{\frac{-2m-1}{2}}\,\Gamma\left(\frac{2m+1}{2}\right){}_2F_1\left(\frac{1}{2}, \frac{2m+1}{2}; \frac{3}{2}; -\frac{sin^2\left(\frac{\pi}{M}\right)}{\mu_{\mathcal{AR}}}\right)\right). \tag{28}$$

$$\alpha_{\mathcal{RB}} = \frac{\delta}{2}\left(1 - 2\sum_{i=0}^{kD-1}\sum_{j=0}^{kD-1} \mathbb{R}_{ij}\sqrt{\frac{\varpi}{\pi}}\,\mu_{\mathcal{RB}}^{\frac{-2m-1}{2}}\,\Gamma\left(\frac{2m+1}{2}\right){}_2F_1\left(\frac{1}{2}, \frac{2m+1}{2}; \frac{3}{2}; -\frac{sin^2\left(\frac{\pi}{M}\right)}{\mu_{\mathcal{RB}}}\right)\right). \tag{29}$$

B. OUTAGE PROBABILITY ANALYSIS

The OP is a measure of how often the overall SNR in a system falls below a specific threshold due to channel effects. It can be represented mathematically as follows

$$\mathbb{P}_{out} = \Pr.\big(\gamma \leq \gamma_{\text{th}}\big). \tag{30}$$

In the considered TWR mmWave-based aerial link system, the average OP at node $\mathcal{A}$ or node $\mathcal{B}$ is identical. Hence, the OP analysis can be computed on only one node, say node $\mathcal{B}$, and it can be expressed as follows

$$\mathbb{P}_{out} = \Pr\{\min\{\gamma_{\mathcal{AR}}, \gamma_{\mathcal{RB}}\} \leq \gamma_{th}\}, \tag{31}$$

where $\gamma_{\mathcal{AR}}, \gamma_{\mathcal{RB}}$ are the SNR for the $\mathcal{A}-\mathcal{R}$, and $\mathcal{R}-\mathcal{B}$ links, respectively. Assuming that $\gamma_{min} = \min\{\gamma_{\mathcal{AR}}, \gamma_{\mathcal{RB}}\}$, the OP can be expressed in terms of CDF as follows

$$\mathbb{P}_{out} = F_{\gamma_{min}}(\gamma_{th}), \tag{32}$$

where $F_{\gamma_{min}}(\gamma)$ is the CDF of γ_{min}, and it can be obtained as follows [30]

$$F_{\gamma_{min}}(\gamma) = F_{\gamma_{\mathcal{AR}}}(\gamma) + F_{\gamma_{\mathcal{RB}}}(\gamma) - F_{\gamma_{\mathcal{AR}}}(\gamma) * F_{\gamma_{\mathcal{RB}}}(\gamma). \tag{33}$$

The OP for the kl link can be derived by calculating the CDF of the RV γ_{kl} using (24), and [31, eq. (8.350.1)] as follows

$$F_{\gamma_{kl}}(\gamma_{kl}) = \sum_{i=0}^{kD-1}\sum_{j=0}^{kD-1} \mathbb{R}_{ij}\,\mu_{kl}^{m} \times \mathcal{V}\left(m, \frac{m\,\sigma^2}{P\,\rho_{kl}\mathbb{R}_{ij}}\gamma_{kl}\right), \tag{34}$$

where $\mathcal{V}(.,.)$ is an incomplete Gamma function. Hence, the OP at node $\mathcal{B}$ can be expressed in (35) at the bottom of the page by substituting (34) into (33).

VI. SIMULATION RESULTS

This section presents a comprehensive evaluation of the TWR mmWave-based aerial communication system. Through a combination of simulations and analytical formulas, we assess the system performance and reliability. The simulations provide practical evidence, while the analytical approach offers valuable theoretical insights. The simulations parameters that are fixed are listed in Table 1.

In Fig. 4, the average BER performance of the considered dual-hop TWR mmWave-based aerial links is explored considering different operational parameters. In Fig. 4-(a), the influence of varying the modulation order within the studied system is depicted. Notably, increasing the modulation order leads to a negative impact on the BER performance within mmWave-based aerial communication scenarios. This outcome signifies that employing higher modulation order results in higher probabilities of errors during data transmission. Moreover, the matching between the analytical and simulation results is distinctly evident, underscoring the precision of the derived closed-form expressions.

TABLE 1. Parameters for simulation results.

Parameter	Value	Parameter	Value
σ^2	-110 dBm	m	3
F_m	30	G_{SL}	30
h	30m	G_{max}	10dBi
θ_{e3dB}	65°	ϕ_{e3dB}	65°
f_c	50 GHz	D	4
θ'_{kx}	$0.2 \times 10^{-3^\circ}$	θ'_{ky}	$0.2 \times 10^{-3^\circ}$

In the investigated dual-hop setup, the separation between the UAVs plays a crucial role in determining the BER performance. As indicated in Fig. 4-(b), where the variable d denotes the distance between $\mathcal{A}-\mathcal{R}$ or $\mathcal{R}-\mathcal{B}$. As the UAVs are positioned closer together, the signal strength becomes stronger, resulting in a lower BER and enhanced communication effectiveness. However, as the distance between UAVs expands, the signal strength diminishes, leading to an increased BER and decreased data reliability. By examining how the BER changes across different distances, we gain insights into designing a more effective model for successful communication within mmWave-based UAV networks.

The number of antenna elements in UAVs has a significant impact on the BER in TWR mmWave-based aerial communication. As visualized in Fig. 4-(c), as the number of antenna elements increases, the system's beamforming capabilities improves, allowing for more precise and focused signal transmission and reception. This increased beamforming ability enhances the directivity of the antennas, concentrating the transmitted power towards the intended direction and increasing the received signal power at the destination UAV's node. Hence, the BER decreases as the number of antenna elements increases.

The instability factor of UAVs σ_θ^2, which refers to the random fluctuations in the antennas during communication, can significantly impact the BER performance in TWR mmWave-based aerial communication system. When UAVs experience higher instability, their positions may vary more rapidly, leading to changes in the link quality. As a result, the received signal strength will fluctuate, affecting the overall communication performance. As visualized in Fig. 4-(d), as

$$\mathbb{P}_{out}^{\mathcal{B}} = \sum_{i=0}^{kD-1}\sum_{j=0}^{kD-1} \frac{\mathbb{R}_{ij}}{\mu_{\mathcal{AR}}^{m}} \times \mathcal{V}(m, \mu_{\mathcal{AR}}\,\gamma_{\mathcal{AR}}) + \sum_{i=0}^{kD-1}\sum_{j=0}^{kD-1} \frac{\mathbb{R}_{ij}}{\mu_{\mathcal{RB}}^{m}} \times \mathcal{V}(m, \mu_{\mathcal{RB}}\,\gamma_{\mathcal{RB}}) - \left(\sum_{i=0}^{kD-1}\sum_{j=0}^{kD-1} \frac{\mathbb{R}_{ij}}{\mu_{\mathcal{AR}}^{m}} \times \mathcal{V}(m, \mu_{\mathcal{AR}}\,\gamma_{\mathcal{AR}})\right)\left(\sum_{i=0}^{kD-1}\sum_{j=0}^{kD-1} \frac{\mathbb{R}_{ij}}{\mu_{\mathcal{RB}}^{m}} \times \mathcal{V}(m, \mu_{\mathcal{RB}}\,\gamma_{\mathcal{RB}})\right). \tag{35}$$

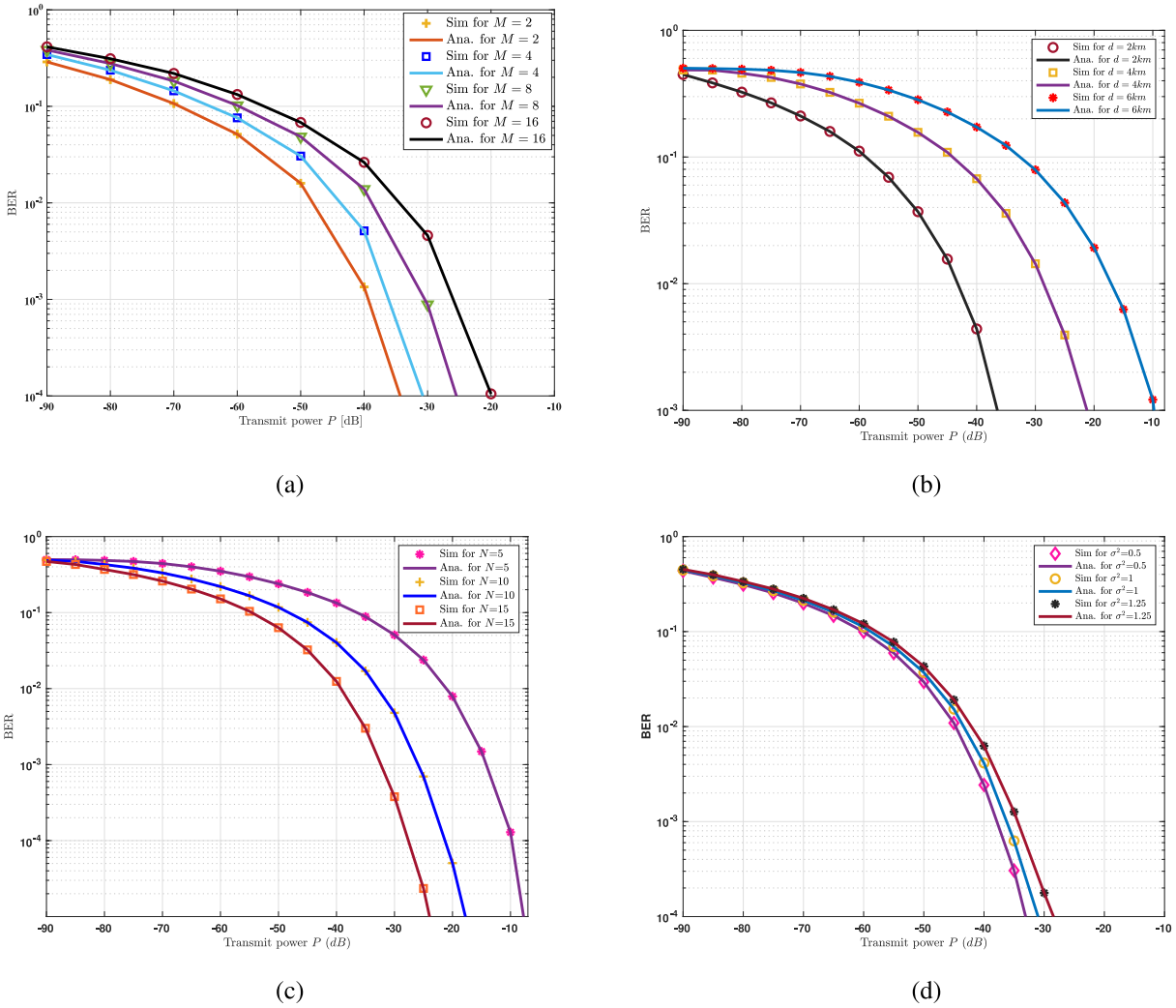

FIGURE 4. The average BER versus the transmit power of dual-hop TWR mmWave-based aerial system at (a) different values of modulation order M ($N = 20$, $\sigma_\theta^2 = 1$, $d = 2Km$), (b) different values of distances between nodes d ($N = 20$, $\sigma_\theta^2 = 1°$, $M = 8$), (c) different values of antenna elements N ($M = 8$, $\sigma_\theta^2 = 1°$, $d = 2Km$), and (d) different values of UAV's fluctuation intensity σ_θ^2 ($N = 20$, $M = 8$, $d = 2Km$).

the UAV's instability factor increases from $\sigma_\theta^2 = 0.5°$ to $\sigma_\theta^2 = 1.25°$, the BER tends to rise due to the increases in the probability of communication errors caused by signal fluctuations and misalignment between antennas beams. Therefore, minimizing UAV instability becomes crucial to ensure reliable and stable communication.

The OP of the investigated system is studied in Fig. 5 considering different operational parameters. The relationship between the SNR threshold and the OP in the studied system is shown in Fig. 5-(a). A notable trend is observed: as the SNR threshold increases, there is a simultaneous increase in the OP. To elaborate, when a higher signal quality is required for successful communication by increasing the SNR threshold, the OP also increases. This indicates that, a stricter SNR threshold might reduce the overall reliability of the system, resulting in a higher likelihood of communication outage.

The influence of the distance between nodes on the OP within the investigated system is presented in Fig. 5-(b). The graph demonstrates a clear trend: as the distance between nodes increases, the OP tends to increase as well. This observation highlights the crucial role of node spacing in determining the system's performance. Specifically, maintaining a sufficient distance between nodes contributes to reducing the chances of signal degradation due to path loss and other propagation effects.

Fig. 5-(c) vividly demonstrates the relationship between the number of antenna elements and the OP of the TWR mmWave-based aerial communication system. This visual aid illustrates that increasing the number of antenna elements corresponds to a lower OP. This emphasizes the significance of how the antenna design plays in enhancing the performance, and minimizing outages in the investigated communication systems.

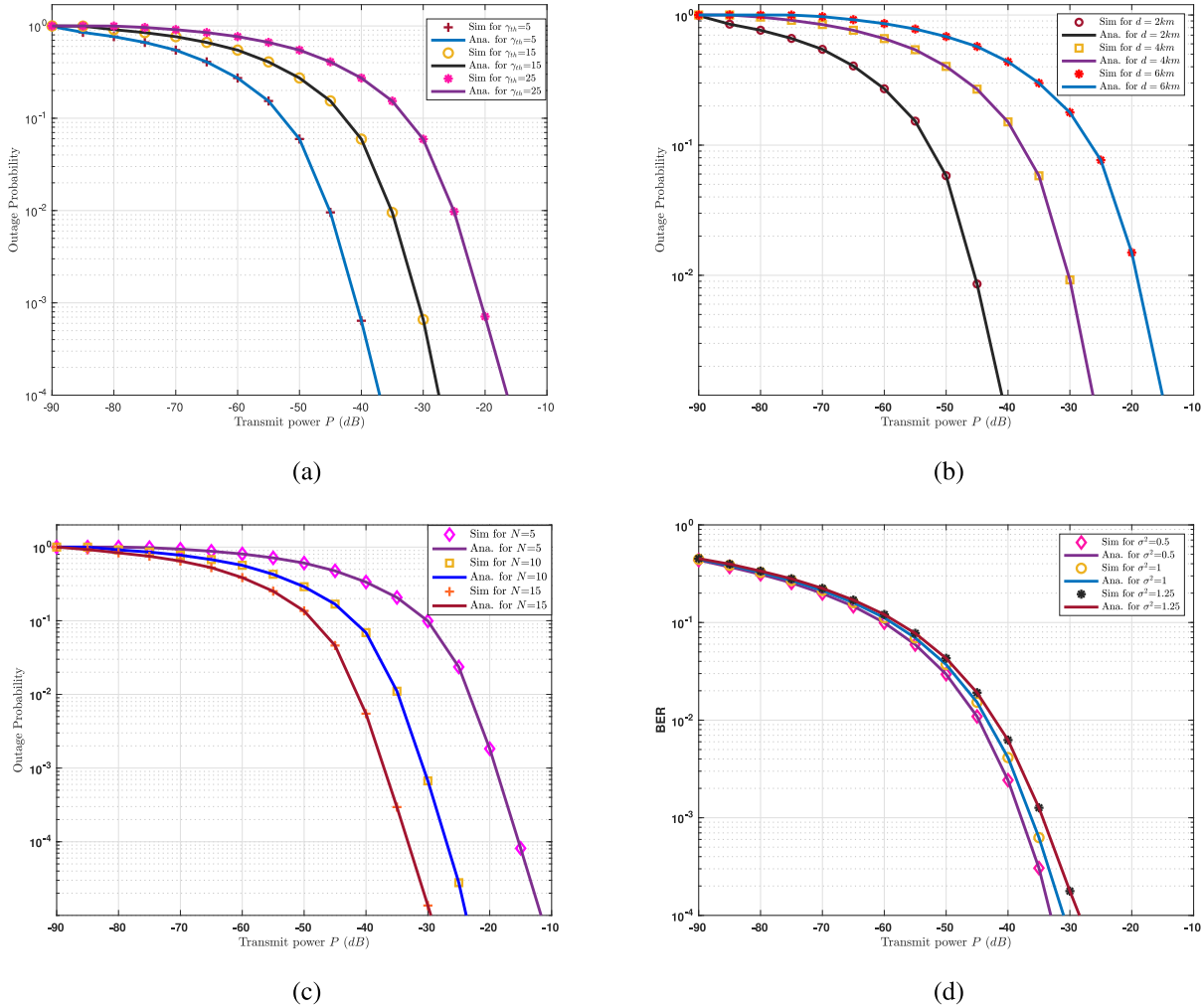

FIGURE 5. The average outage probability versus the transmit power of dual-hop TWR mmWave-based aerial system at (a) different values of the SNR threshold $\gamma_{\rm th}$ ($N = 20$, $M = 8$, $\sigma_\theta^2 = 1°$, $d = 2Km$), (b) different values of distances between nodes d ($N = 20$, $M = 8$, $\sigma_\theta^2 = 1°$,$d = 2Km$, and $\gamma_{\rm th} = 5$), (c) different values of antenna elements N ($M = 8$, $\sigma_\theta^2 = 1°$, $d = 2Km$, $\gamma_{\rm th} = 5$), and (d) different values of UAV's fluctuation intensity σ_θ^2 ($N = 20$, $M = 8$, $d = 2Km$, $\gamma_{\rm th} = 5$).

Furthermore, Fig. 5-(d) sheds light on the impact of the UAV's instability parameter on the OP within the studied system. This illustration offers a clear understanding of how varying the UAV's fluctuation parameter can influence the likelihood of communication outages. As the UAV's fluctuation parameter increases, the OP tends to rise.

VII. CONCLUSION

The performance of TWR in mmWave-based aerial links has been addressed in this paper in terms of the error analysis, and OP. The system under investigation involves three UAVs, where two of them are exchanged data while the third UAV acts as a relay. The performance has been analyzed while considering the impact of the fluctuations in the antenna orientation of all aerial nodes that are caused by the vibration of the hovering UAVs. Furthermore, comprehensive analysis has been conducted, successfully yielding closed-form expressions for the average BER and OP. These analytical findings have been shown to closely align with simulation results. Through extensive investigation, the performance of the TWR system is assessed across various factors, including the distance between nodes, the number of antenna elements, UAV vibration intensity and modulation order.

ACKNOWLEDGMENT

The statements made herein are solely the responsibility of the authors.

REFERENCES

[1] K. Aldubaikhy, W. Wu, N. Zhang, N. Cheng, and X. Shen, "mmWave IEEE 802.11ay for 5G fixed wireless access," *IEEE Wireless Commun.*, vol. 27, no. 2, pp. 88–95, Apr. 2020.

[2] L. Zhu, J. Zhang, Z. Xiao, X. Cao, X.-G. Xia, and R. Schober, "Millimeter-wave full-duplex UAV relay: Joint positioning, beamforming, and power control," *IEEE J. Sel. Areas Commun.*, vol. 38, no. 9, pp. 2057–2073, Sep. 2020.

[3] L. Bai, Z. Huang, L. Cui, and X. Cheng, "A non-stationary multi-UAV cooperative channel model for 6G massive MIMO mmWave communications," *IEEE Trans. Wireless Commun.*, vol. 22, no. 12, pp. 9233–9247, Dec. 2023.

[4] M. Awad, S. M. Ibraheem, S. A. Napoleon, W. Saad, M. Shokair, and M. E. Nasr, "Secrecy enhancement of cooperative NOMA networks with two-way untrusted relaying," *IEEE Access*, vol. 8, pp. 216349–216364, 2020.

[5] Z. He, H. Shen, W. Xu, and C. Zhao, "Energy efficient joint power optimization for full-duplex relaying," *IEEE Access*, vol. 7, pp. 137040–137047, 2019.
[6] N. Zhao et al., "UAV-assisted emergency networks in disasters," *IEEE Wireless Commun.*, vol. 26, no. 1, pp. 45–51, Feb. 2019.
[7] Z. Xiao, L. Zhu, and X.-G. Xia, "UAV communications with millimeter-wave beamforming: Potentials, scenarios, and challenges," *China Commun.*, vol. 17, no. 9, pp. 147–166, Sep. 2020.
[8] K. Belbase, C. Tellambura, and H. Jiang, "Two-way relay selection for millimeter wave networks," *IEEE Commun. Lett.*, vol. 22, no. 1, pp. 201–204, Jan. 2018.
[9] S. Gong, C. Xing, Z. Fei, and S. Ma, "Millimeter-wave secrecy beamforming designs for two-way amplify-and-forward MIMO relaying networks," *IEEE Trans. Veh. Technol.*, vol. 66, no. 3, pp. 2059–2071, Mar. 2017.
[10] S. Bera, S. Chakraborty, D. Sen, and A. K. Dutta, "Iterative variational Bayesian inference based channel estimation for TWR mmWave systems," *IEEE Trans. Veh. Technol.*, vol. 72, no. 8, pp. 10330–10344, Aug. 2023.
[11] Z. Sheng, H. D. Tuan, T. Q. Duong, and L. Hanzo, "UAV-aided two-way multi-user relaying," *IEEE Trans. Commun.*, vol. 69, no. 1, pp. 246–260, Jan. 2021.
[12] X. Guo, B. Li, J. Cong, and R. Zhang, "Throughput maximization of a UAV-enabled two-way relaying system," in *Proc. IEEE Int. Conf. Commun.*, Montreal, QC, Canada, 2021, pp. 1–6.
[13] B. Li, S. Zhao, R. Zhang, and L. Yang, "Joint transmit power and trajectory optimization for two-way multihop UAV relaying networks," *IEEE Internet Things J.*, vol. 9, no. 23, pp. 24417–24428, Dec. 2022.
[14] S. Wang, L. Li, R. Ruby, X. Ruan, J. Zhang, and Y. Zhang, "Secrecy-energy-efficiency maximization for UAV-enabled two-way relay systems," *IEEE Trans. Veh. Technol.*, vol. 72, no. 10, pp. 12900–12911, Oct. 2023.
[15] M. N. Bashir, K. M. Yusof, and S. Iqbal, "Outage performance analysis of UAV-assisted dual-hop cooperative network under distortions and interferences," in *Proc. 8th Int. Conf. Inf. Technol. Trends (ITT)*, Dubai, UAE, 2022, pp. 45–50.
[16] R. D. Govenker, A. Y. Phatak, R. Bajpai, and N. Gupta, "Outage analysis of mmWave integrated device-to-device communication system under Nakagami fading channel," in *Proc. Nat. Conf. Commun. (NCC)*, Kharagpur, India, 2020, pp. 1–6.
[17] M. T. Dabiri, M. Rezaee, V. Yazdanian, B. Maham, W. Saad, and C. S. Hong, "3D channel characterization and performance analysis of UAV-assisted millimeter wave links," *IEEE Trans. Wireless Commun.*, vol. 20, no. 1, pp. 110–125, Jan. 2021.
[18] M. Mozaffari, W. Saad, M. Bennis, and M. Debbah, "Communications and control for wireless drone-based antenna array," *IEEE Trans. Commun.*, vol. 67, no. 1, pp. 820–834, Jan. 2019.
[19] J. Wang, C. Jiang, Z. Wei, C. Pan, H. Zhang, and Y. Ren, "Joint UAV hovering altitude and power control for space-air-ground IoT networks," *IEEE Internet Things J.*, vol. 6, no. 2, pp. 1741–1753, Apr. 2019.
[20] M. Mozaffari, W. Saad, M. Bennis, and M. Debbah, "Wireless communication using unmanned aerial vehicles (UAVs): Optimal transport theory for hover time optimization," *IEEE Trans. Wireless Commun.*, vol. 16, no. 12, pp. 8052–8066, Dec. 2017.
[21] H.-T. Ye, X. Kang, J. Joung, and Y.-C. Liang, "Optimization for full-duplex rotary-wing UAV-enabled wireless-powered IoT networks," *IEEE Trans. Wireless Commun.*, vol. 19, no. 7, pp. 5057–5072, Jul. 2020.
[22] S. G. Sanchez, S. Mohanti, D. Jaisinghani, and K. R. Chowdhury, "Millimeter-wave base stations in the sky: An experimental study of UAV-to-ground communications," *IEEE Trans. Mobile Comput.*, vol. 21, no. 2, pp. 644–662, Feb. 2022.
[23] *Technical Specification Group Radio Access Network; Study of Radio Frequency (RF) and Electromagnetic Compatibility (EMC) Requirements for Active Antenna Array System (AAS) Base Station*, 3GPP Standard 37.840, 2013.
[24] C. A. Balanis, *Antenna Theory: Analysis and Design*. Newark, NJ, USA: Wiley, 2016.
[25] "Study on channel model for frequencies from 0.5 to 100 GHz (Release 16)," 3GPP, Sophia Antipolis, France, Rep. 3GPP TR 38.901, V14.1.1, 2020.
[26] N. Goddemeier and C. Wietfeld, "Investigation of air-to-air channel characteristics and a UAV specific extension to the rice model," in *Proc. IEEE Globecom Workshops (GC Wkshps)*, San Diego, CA, USA, 2015, pp. 1–5.
[27] R. van Nee, A. van Zelst, and G. Awater, "Maximum likelihood decoding in a space division multiplexing system," in *Proc. IEEE 51st Veh. Technol. Conf.*, vol. 1, Tokyo, Japan, 2000, pp. 6–10.
[28] O. S. Badarneh and R. Mesleh, "Diversity analysis of simultaneous mmWave and free-space-optical transmission over F-distribution channel models," *J. Opt. Commun. Netw.*, vol. 12, no. 11, pp. 324–334, Nov. 2020.
[29] E. W. Ng and M. Geller, "Table of integrals of the error functions," *J. Res. Nat. Bur. Stand. B, Math. Sci.*, vol. 73B, no. 1, pp. 1–20, Jan.–Mar. 1969.
[30] A. Papoulis and S. U. Pillai, *Probability, Random Variables and Stochastic Processes*. New York, NY, USA: McGraw-Hill, 2002.
[31] A. Jeffrey and D. Zwellinger, *Table of Integrals, Series, and Products*. Burlington, MA, USA: Elsevier, 2007.

HEYAM F. HASSAN received the B.Sc. degree in electrical engineering from Qatar University in 2020. She is currently working as a Research Assistant with the Department of Electrical and Computer Engineering, Texas A&M University at Qatar. Her research interests include millimeter wave and terahertz communications, wireless communications, nonorthogonal multiple access, and cooperative networks.

SAUD ALTHUNIBAT (Senior Member, IEEE) received the Ph.D. degree in telecommunications from the University of Trento, Trento, Italy, in 2014. He is currently a Professor with the Department of Communications Engineering, Al-Hussein Bin Talal University, Ma'an, Jordan. He is also with the Department of Electrical and Computer Engineering, Texas A&M University at Qatar as a Research Scientist. He has authored more than 130 scientific papers. He is the General CoChair of BROADNETs 2018 conference. His research interests include a wide range of wireless communication topics such as, index modulation, spectrum sharing, cognitive radio, wireless sensor networks, energy efficiency, and resource allocation. He was the recipient of the Best Paper Awards in IEEE CAMAD 2012 and IEEE Globecom 2022, and was selected as an Exemplary Reviewer for the IEEE COMMUNICATION LETTERS in 2013. He was the recipient of the Distinguished Researcher Award granted by Hamdi Mango Center—The University of Jordan in 2022. He served as an Editor in IEEE COMMUNICATION LETTERS.

MOHAMMAD TAGHI DABIRI received the Ph.D. degree (Hons.) in electrical engineering (telecommunications) from Shahid Beheshti University, Tehran, Iran, in 2018. From 2018 to 2021, he worked with the IRAN Telecommunication Research Center. He is currently a Postdoctoral Fellow with Qatar University, Doha, Qatar. His main research interests include wireless communications focusing on indoor optical wireless communications, outdoor free-space optical communications, mmWave/THz communications, unmanned aerial vehicles communications, satellite communications, non-terrestrial network design, synchronization and detection theory, light detection and ranging, tracking and alignment techniques, channel modeling, intelligent networks, and reinforcement learning.

MAZEN HASNA (Senior Member, IEEE) received the B.S. degree in electrical engineering from Qatar University, Doha, Qatar, in 1994, the M.Sc. degree in electrical engineering from the University of Southern California, Los Angeles, CA, USA, in 1998, and the Ph.D. degree in electrical engineering from the University of Minnesota Twin Cities, Minneapolis, MN, USA, in 2003. In 2003, he joined the Staff of the Electrical Engineering Department, Qatar University, where he is currently a Professor of Communications. From 2005 to 2017, he was with several administrative capacities within Qatar University, including the Head of Electrical Engineering Department, Dean of the College of Engineering, and VPCAO. His research interests include the application of digital communication theory to the performance analysis of wireless communication systems, aerial networks, D2D enabled communications, physical-layer security, FSO/RF hybrid networks, and RIS-based communications. He is listed in the 2015 Highly Cited Researchers List of Clarivate Analytics, and has received research grants in the last ten years worth of more than 5M, both from industry and government. He co-founded and also serves on the Joint Management Committee with Qatar Mobility Innovation Center, an innovation center promoting using research and development to develop and deploy intelligent mobility and smart cities platforms and technologies. He is a Founding Member of the IEEE Qatar Section and was its founding VP.

KHALID A. QARAQE (Senior Member, IEEE) was born in Bethlehem. He received the B.S. (Hons.) degree in electrical engineering from the University of Technology, Bagdad, Iraq, in 1986, the M.S. degree in electrical engineering from the University of Jordan, Amman, Jordan, in 1989, and the Ph.D. degree in electrical engineering from Texas A&M University at College Station, College Station, TX, USA, in 1997. From 1989 to 2004, he has held a variety positions in many companies and he has over 12 years of experience in the telecommunication industry. He has worked on numerous projects and has experience in product development, design, deployments, testing, and integration. He joined the Department of Electrical and Computer Engineering, Texas A&M University at Qatar, Qatar, in July 2004, where he is currently a Professor and the Managing Director with the Center for Remote Healthcare Technology, Qatar. He has been awarded more than 20 research projects consisting of more than USD 13M from local industries in Qatar and the Qatar National Research Foundation. He has published more than 131 journal papers in top IEEE journals, and published and presented 250 papers at prestigious international conferences. He has 20 book chapters published, four books, three patents, and presented several tutorials and talks. His research interests include communication theory and its application to design and performance, analysis of cellular systems and indoor communication systems. Particular interests are in mobile networks, broadband wireless access, cooperative networks, cognitive radio, diversity techniques, index modulation, visible light communication, FSO, tele-health, and noninvasive bio sensors. He received the Itochu Professorship Award in 2013–2015, the Best Researcher Award from QNRF 2013, the Best Paper Award from the IEEE First Workshop on Smart Grid and Renewable Energy in 2015, the Best Paper Award from the IEEE Globecom 2014, the Best Poster Award IEEE Dyspan Conference in 2012, the TAMUQ Research Excellence Award in 2010, the Best Paper Award from ComNet in 2010, the Best Paper Award from CROWNCOM in 2009, the Best Paper Award from the ICSPC'0 in 2007, the IEEE Signal Processing Magazine Best Column Award in 2018, the Best Oral Presentation Award from CECNet 2018, the Best Paper Award, Green Communications, Computing and Technologies Conference in 2016, Faculty of the Year (Student Award) in 2016 and 2015, and the Best Faculty Award by the student body in 2015.